scientific reports

Check for updates

OPEN

Effects of wind turbine wakes on bird gliding aerodynamic performance

Xuefeng Yang[1,2], Lifan Zhou[1,2], Yi Sui[1], Zhengru Ren[1] & Shengli Chen[1]✉

Wind power, as a critical source of renewable energy to combat global warming, is growing rapidly worldwide. A great concern has arisen over the killing of a great number of birds by wind turbines. There has been much research on this issue based on observational and statistical data. However, it remains unknown how the wind turbine wakes affect the bird flight from a fluid dynamic and mechanical perspective. The wind turbine wakes calculated by the large eddy simulation are used as boundary input to simulate the flying of bird. A number of 62 bird flight simulations are run to calculate the lift-to-drag ratio, and then fitted to get its distribution over the whole wake area. Results reveal bird flights are affected most near the upper blade tip, with a maximum reduction in lift-to-drag ratio of about 30%. Conversely, turbine wakes below bottom tip level assist bird flight, suggesting a potential low-altitude route through wind farms. Wake superposition exacerbates adverse aerodynamic effects, and a staggered layout strategy can reduce the negative impact. The findings will benefit the conservation of birds and assist the sustainable development of wind farms.

Keywords Bird flight, Turbine wake, Numerical simulation

Wind energy is an increasingly pivotal role in the context of accelerating development of new energy sources. In 2023, the global wind power industry increased by 50% from 2022, with a new installed capacity of 117 GW[1]. The rapid development of the wind power industry also has increasing impacts on the surrounding ecology, particularly with regard to the flight safety of birds[2,3]. The number of birds that die annually as a result of wind farms is considerable. In U. S, the estimated annual mortality of birds from collisions with wind turbines ranges from 234,000 to 573,000[4–7]. These make wind power the most threatening form of green energy to birds. Although some researchers maintain that birds can adapt to wind farms and the construction of wind farms will not result in a notable increase in bird-aircraft collisions, the precise duration for such adaptation remains uncertain. It is therefore evident that until this adaptation is complete, there is a necessity for further attempts and efforts to ensure the safety of birds in flight[8,9].

Substantial research has investigated factors influencing bird collisions with turbines. From the perspective of a wind farm, the probability of bird collision is influenced by the location of the turbines[10], topographic conditions[11], design features and the layout of the wind farm[12,13]. From the perspective of the bird, factors include the species[14], seasonal migration patterns[15], the flight height[16], and whether it is flocking[17,18]. Some scholars have examined the impact of wind farms on bird flight behaviour. The presence of wind turbines has been observed to promote certain birds to select less energy-intensive flight paths[19]. And large birds have been documented to exhibit avoidance behaviors in the presence of large wind turbines, both vertically and horizontally[20]. Furthermore, efforts have been made to ascertain methods for reducing the likelihood of bird collisions on wind turbines. A numerical model has been developed to assess the risk and mortality of bird collisions with wind turbines[21]. The painting of wind turbine tower bases can markedly reduce the incidence of collisions[22]. Despite these efforts, turbine-induced bird collisions remain a significant challenge.

Previous studies demonstrate the significant impact of the wind farms on the bird flight, which are mostly based on statistics data of bird. The impacts are presumably attributed to the irregular and turbulent flow behind the wind turbine. However, little is understood on how the turbine wake works on the bird flying in perspective of aerodynamic performance. Knowledge of this issue is fundamental, generalized, and could benefit a lot in the sustainable development of wind energy. This paper uses large eddy simulation (LES) to calculate the velocity and the turbulence intensity of the wind turbine wakes, which are set as the incoming flow field for the microscopic-scale Reynolds-averaged Navier-Stokes equations (RANS) simulation of bird flight. This study proposes a computationally efficient, decoupled CFD framework to map the baseline aerodynamic perturbations

[1]Institute for Ocean Engineering, Shenzhen International Graduate School, Tsinghua University, Shenzhen 518055, China. [2]Xuefeng Yang and Lifan Zhou contributed equally to this work. ✉email: shenglichen@sz.tsinghua.edu.cn

within a wind turbine wake. A static, gliding bird model is employed as a reference aerodynamic body, providing a foundational assessment prior to modeling more complex, active flight behaviors.

Results

2 MW wind turbines, which is commonly employed in scientific research[25–28], utilized has a swept diameter of about 80 m, whereas the typical bird flight assumes a wingspan of less than 2 m. This discrepancy in the flow scales is notable. It is not feasible to perform both numerical simulations of the turbine wake and the bird flying using the same grid setting, as this would consume substantial computational resources. Considering their scale difference, we choose LES to simulate the turbine wake, subsequently extract the flow field (including wind speed and turbulence intensity) at the corresponding locations as input boundary conditions for the RANS simulation of the bird flight. In the bird flight simulation, the bird is in a headwind gliding state (relative speed to the ground is zero). This setup enables us to calculate the lift-to-drag ratio of bird flight and study its flight aerodynamic performance at different locations of the turbine wake.

Modelling the bird flight in the turbine wake

The flow field data are extracted along the vertical (z-axis) and horizontal (x-axis) directions, respectively (Fig. 1). A more extensive selection of points would be preferable to account for the asymmetric wake characteristics induced by turbine rotation and the flow field alterations in upper layers resulting from wake expansion. However, due to computational resource limitations, we adopted the current scheme, which can cover most combinations of wind speed and turbulence intensity scenarios. The extracted data will be used for the boundary conditions for the bird flight simulation, to calculate the lift, drag, and lift-to-drag ratios of the birds (Fig. 2).

The variation of the lift-to-drag ratio (K) displays an obvious dependence with height (Fig. 2a, b). The K is smallest (≈ 4) at the position of the top tip level, indicating the greatest negative impact on the bird flying. Above the top tip, K gradually rises with height, reaching a maximum value of 6.6 at the highest position. Below the top tip, K similarly rises, achieving a local maximum (5.5) at hub height. Underneath the hub, K only has small variation. It is 5.0 at the sea surface, and has a slight rise until the bottom tip height.

K comparisons upstream and downstream reveal significant differences (Fig. 2b), confirming that the aerodynamic performance of bird flight is indeed influenced by the wind turbine wakes. K is mostly reduced under the influence of the wind turbine. The reduction is greatest at the top tip level. As the height increases, the difference in K almost vanishes at the height of 160 m. From sea level to the bottom tip, the K is slightly larger under the influence of wind turbine. This means the presence of wind turbine wake assists the bird flight in this region.

Along the downstream direction, the K also shows some variation (Fig. 2c). In general, the K values at all three heights demonstrate a gradual decline in the streamwise direction. This is primarily attributable to the incremental escalation in wake turbulence intensity along the flow direction. At the heights of the bottom tip and top tip, it declines quickly behind the wind turbine, and reaches a minimum value at the 3 D position, behind

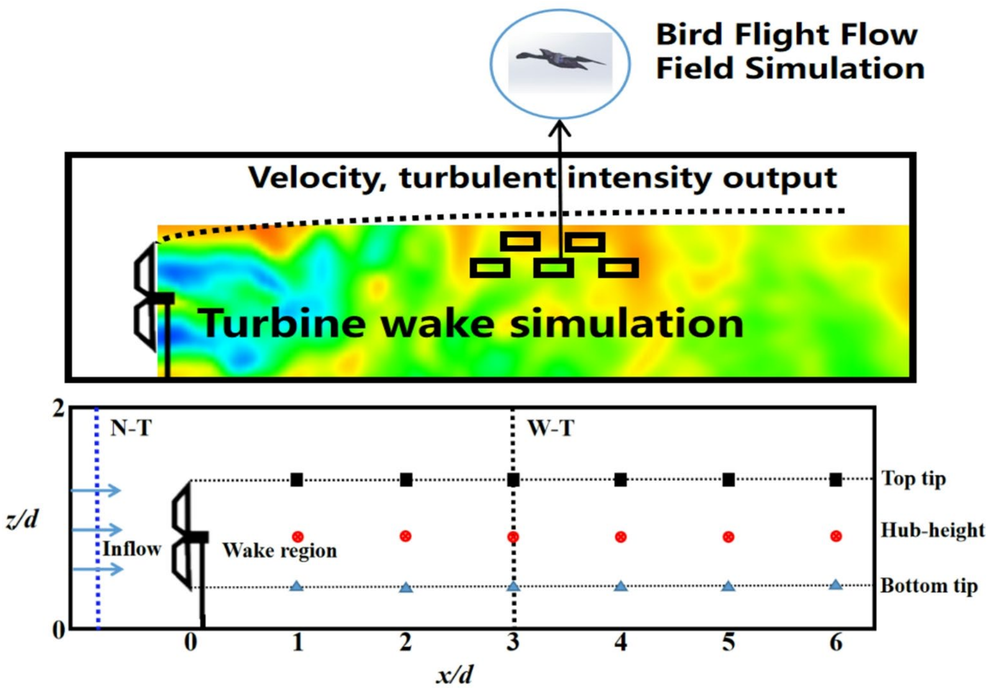

Fig. 1. Schematic of the computational domain of the wind turbine flow field with the locations of the selected points for the bird flight simulations (62 in total): the two dashed lines N-T and W-T (22 each), the top tip, the hub height and the bottom tip (6 each).

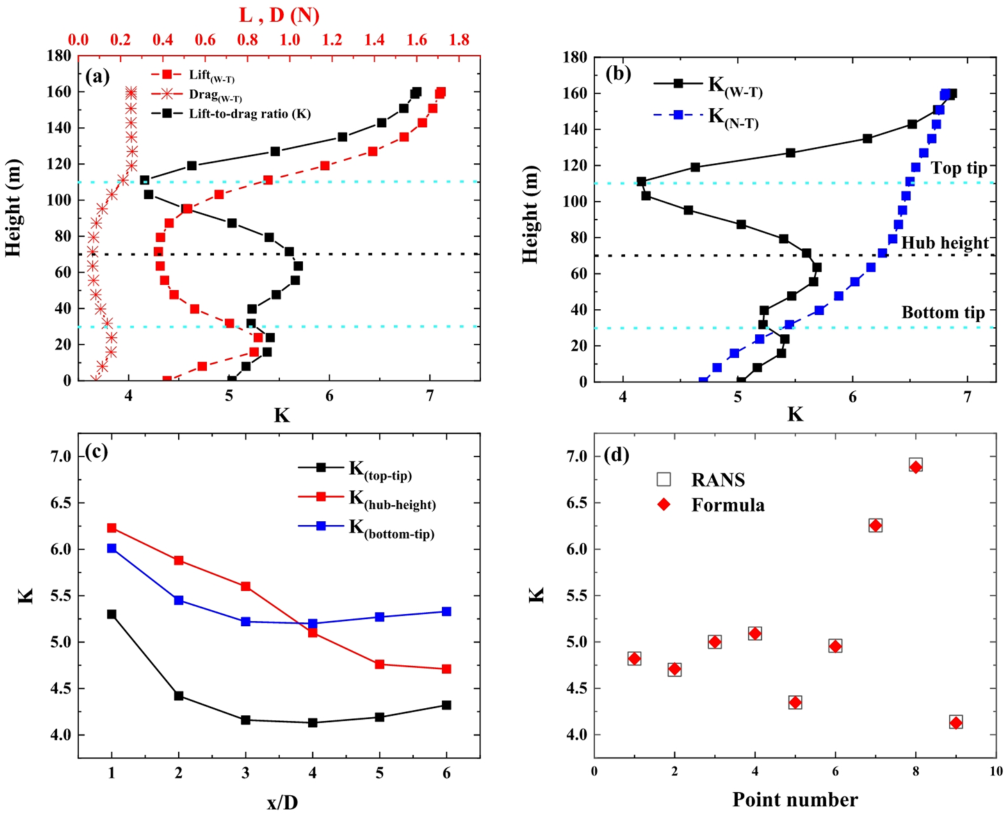

Fig. 2. (a) Lift, drag, and the lift-to-drag ratio versus height for birds at 3 D in the wake. (b) Lift-to-drag ratio versus height for birds with and without the wind turbine at 3 D in the wake. (c) Lift-to-drag ratio at the top tip level, hub height, and bottom tip level at different distances after the wake. (d) Comparison of experimental values with the predicted values of the fitted function.

which it grows slightly. The ratio at the top tip is always the smallest, suggesting the most pronounced influence on the bird flight. The K is higher at the hub height than at the bottom tip level before 4 D distance. This reverses after 4 D. The wake flow velocity at the hub height undergoes a notable decline prior to 4 D, yet the turbulence intensity remains relatively low, thereby conferring an enhanced K in comparison to the bottom tip (Fig. 2c). However, there is a notable increase in turbulence intensity after 4 D, and turbulence becomes the dominant factor.

A fitting function

Base on the numerical results from the 62 simulation experiments of bird flight, the lift-to-drag ratio (K) is calculated using the wake flow velocity (V) and turbulence intensity (Ti), which is given as,

$$
\begin{aligned}
K = 4.541 + 1.193V - 15.86Ti - 0.1047V^2 - 3.919V \cdot Ti \\
- 159.6Ti^2 + 0.003327V^3 + 0.1907V^2 \cdot Ti \\
- 1.232V \cdot Ti^2 + 1007Ti^3
\end{aligned}
\tag{1}
$$

The functional relationship between the lift-to-drag ratio (K), the incoming streamwise velocity (V), and turbulence intensity (Ti) is established using the Curve Fitting Toolbox in MATLAB R2022a (Fig. S12). A two-variable third-degree polynomial model ('poly33') is employed. The 'poly33' model achieves an exceptional fit to the simulation data, as evidenced by the following goodness-of-fit statistics: a Sum of Squares due to Error (SSE) of 0.001171, a Root Mean Square Error (RMSE) of 0.0048339, and a Coefficient of Determination (R-square) of 0.99997. These metrics confirm that the empirical function reproduces the RANS simulation results with well accuracy within the sampled parameter space of V and Ti.

The validation strategy encompassed nine flow field locations, including four extreme-value points selected to assess predictive accuracy at the boundaries of the sampled parameter space. These points correspond to: (1) minimum wind speed, V = 3.96 m/s; (2) maximum wind speed, V = 8.7 m/s; (3) minimum turbulence intensity, Ti = 5.7%; and (4) maximum turbulence intensity, Ti = 11.9%. These values represent the extremes of wind speed and turbulence intensity observed in the wind turbine wake, as obtained from the large eddy simulation results in Fig. 7. The comparison displayed in Fig. 2d demonstrates the fitting function is highly effective in predicting the K of bird flight within the wake flow field.

Accordingly, the fitted function is applicable over a substantial portion of the wake region. Nevertheless, it is important to emphasize that the empirical model is strictly validated within a defined parameter range. It provides high-fidelity predictions (error < 2%) for conditions with wind speeds below 11 m/s and turbulence intensities below 15%. However, its performance degrades outside this range, with errors exceeding 9% and 37% in high-speed (15 m/s) and high-turbulence (20%) regimes, respectively (Fig. S13). Therefore, the function is recommended for interpolation within its validated bounds of 3–11 m/s for wind speed and 5–15% for turbulence intensity, respectively. Furthermore, the function does not capture the specific, highly unsteady aerodynamic loads imposed by large-scale organized vortical structures, such as the blade tip vortices, which are known to be particularly hazardous.

The analysis indicates that, over the range of conditions studied, the influence of variation in wind speed (V) on the lift-to-drag ratio (K) is substantially smaller than that of turbulence intensity (Ti). Specifically, the analysis reveals a consistent trend: K increases with wind speed but decreases sharply with rising turbulence intensity (Fig. S14).

Effects of single turbine wake

The fitted function are then utilized to extrapolate the impact on bird flight in the full wake region (Figs. 3 and 4). The analysis encompassed the bird flight lift-to-drag ratio, K, at varying positions, in conjunction with the difference, ΔK, subsequent to the subtraction of the bird lift-to-drag ratio at the initial position. Furthermore, in order to quantify the extent to which wind turbine wakes affect bird flight, a dimensionless number, designated $\Delta K/K_0$, is utilized for characterization. The expressions are shown below:

$$\Delta K = K_0 - K \tag{2}$$

$$\Delta K/K_0 = (K_0 - K)/K_0 \tag{3}$$

The results demonstrate that the negative effect on the bird flight is most pronounced at the top tip level (110 m above sea level), irrespective of the distance downstream the turbine. These results are consistent with the numerical study (Fig. 2) of the effects on birds, which attributed this phenomenon to turbulence generated by the turbine at the top tip level. The impact reaches a maximum at approximately 4 D downstream of the turbine (Fig. 3). The wind turbine wakes bring negative influence on the bird flight in most positions, except below the bottom tip level (30 m) where the wind turbine wake assists the flying of bird.

The wake exerts the most pronounced influence on bird flight at a distance of approximately 4 d downstream of the turbine (Fig. 3). Subsequent analyses are conducted at this precise location (Fig. 4). The inverted U-shaped relationship between turbulence intensity and $\Delta K/K_0$ is highly similar, which again confirms that turbulence intensity in the wake has a primary impact on bird flight. Furthermore, the wake at the top tip level has large impact on bird flight, with values of $\Delta K/K_0$ in these regions all exceeding 20%. In contrast, the area below the hub to the lower tip exerts a relatively minor influence. The extensive area below the lower blade tip is largely unperturbed by the wake, exhibiting even a partial increase in K values in this region that slightly assists the bird flight and serves as a 'flight path'. The influence of streamwise velocity is also significant. The positive $\Delta K/K_0$ observed in the wake core region are primarily attributable to velocity deficits, given that turbulence intensity here remains comparable to inflow conditions. Conversely, negative $\Delta K/K_0$ below the bottom tip level result from the combined effects of reduced turbulence intensity and accelerated flow. A comparison of the flight height statistics of common cranes before and after the establishment of wind farms in the literature revealed patterns that support our conclusions (Fig. 4f). The probability of common cranes flying through the height of the turbine's swept area decreased substantially after the construction of the wind farms, but barely decreased near the height of the bottom tip in the swept area. Concurrently, the number of birds flying at the height of 'flight path' increased substantially[23,24]. This phenomenon is consistent with the conclusions of our simulation study. Based on the considerable distance between the majority of measurement points and the turbine, turbine wake

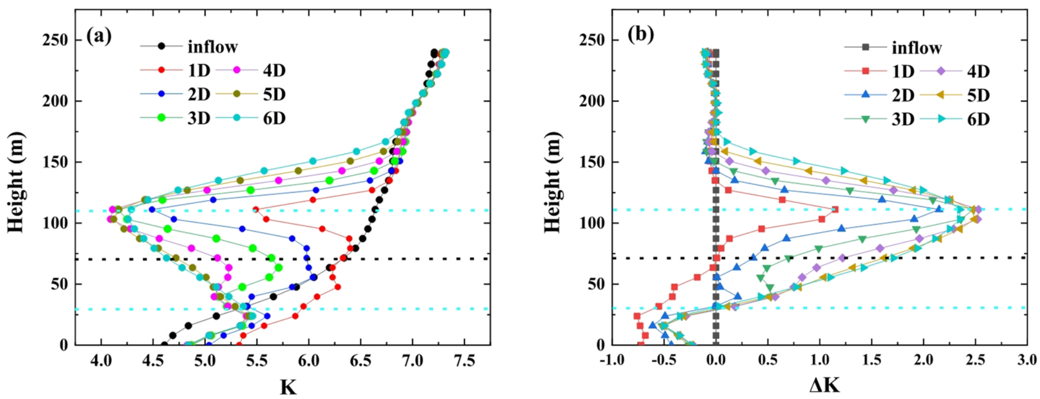

Fig. 3. (a) Lift-to-drag ratio of bird gliding flight at varying distances after wind turbine wakes, (b) the discrepancy in lift-to-drag ratio values (ΔK) between the presence and absence of wind turbines.

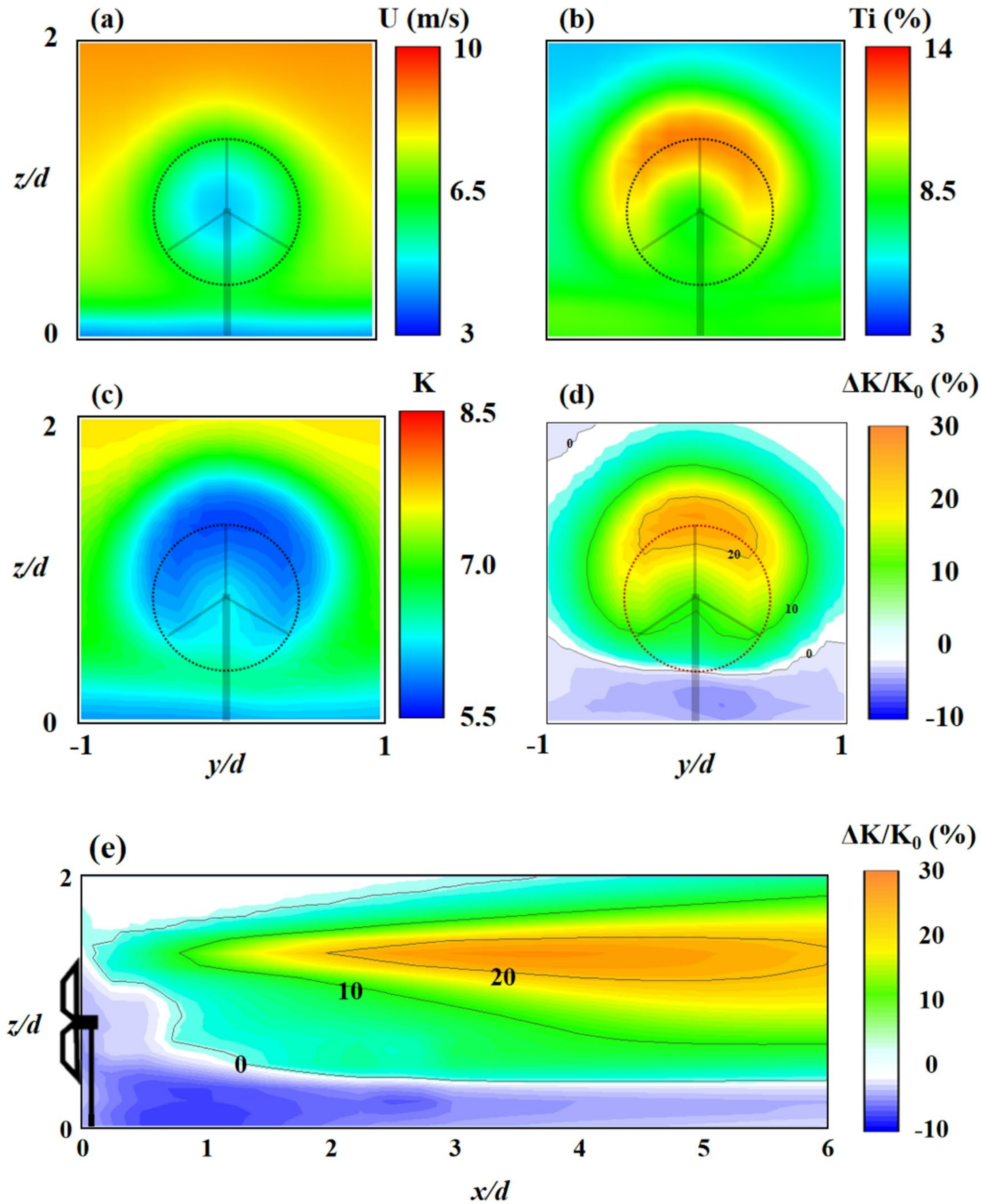

Fig. 4. Distribution of wake-induced mean flow velocity (a), turbulence intensity (b), lift-to-drag ratio (c), and the rate of change of lift-to-drag ratio $\Delta K/K_0$ (d) in the y-z section at 4 d downstream of the wind turbine. The rate of change of lift-to-drag ratio is indicative of the extent to which bird flights are affected. (e) represents the $\Delta K/K_0$ in the centre x-z section. (f) shows the percentage of common cranes at different heights before and after wind farms were built, and the changes[23,24].

is one of the primary factors influencing flight behaviour at this stage, rather than the bird's innate avoidance mechanisms.

Effects of turbine array wake

Since the wind turbine is usually built in array, an investigation is conducted into the impact of multiple turbines wake on bird flight (Fig. 5). The effect of the wake superposition on bird flight is similar to that of the single wake case, with only some minor differences. (1) The extent of the most affected area ($\Delta K/K_0$ > 20%) is much larger than in the single wake case. (2) The favorable passage for bird flights in the stacked wake is narrower than in the

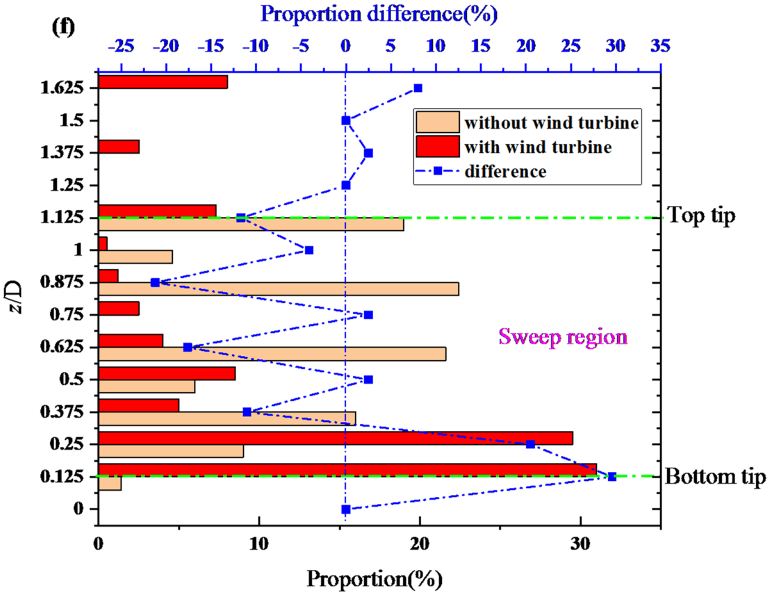

Fig. 4. (continued)

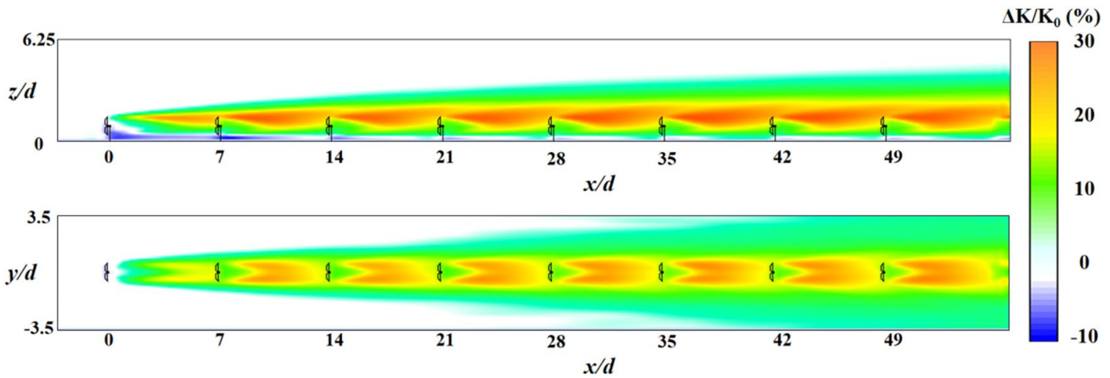

Fig. 5. Distribution of the rate of change of lift-to-drag ratio $|\Delta K/K_0|$ in the centre x-z section and hub-height y-z section in turbine array condition.

single wake case. The primary cause of these phenomena is the additional increase in the turbulence intensity in the wake, which is attributable to the wake superposition effect.

The deployment of comprehensive bird protection systems across entire wind farm domains is impractical from an operational standpoint, given the vast spatial scales involved. a zoning framework is established in order to strategically allocate limited resources for the minimization of wake-induced aerodynamic risks to bird flight. Four functionally distinct zones are defined based on quantified aerodynamic impact ($\Delta K/K_0$):

Hazard Zone (Red): The area exhibits extreme aerodynamic performance reduction, where $\Delta K/K_0 > 20\%$. This critical area corresponds to top tip level, which generate high-intensity turbulent flows. Mandatory eviction measures are required to prevent bird entry.

Surveillance Zone (Yellow/Green): The area exhibits moderate aerodynamic performance reduction ($\Delta K/K_0$ is between 0% and 20%). This region demands adaptive management.

Baseline Zone (White): The area is aerodynamically neutral ($\Delta K/K_0 = 0\%$) beyond the influence of the wake. No active interventions are required within this area, which serves as a reference for monitoring undisturbed flight behaviour.

Flight path (Blue): The area exhibits favourable aerodynamic conditions ($\Delta K/K_0 < 0\%$), which are comprised of two distinct subdomains: (1) Turbine-adjacent zones (0-0.5 D leeward): Despite the enhancement of bird flight aerodynamic effects, the utilization of blade proximity sensors and bird redirection systems remains imperative to avert collision events. (2) Surface flight paths: The wake enhances the aerodynamic performance of bird flight in this area, and no measures are required.

The zoning framework facilitates cost-effective risk stratification while preserving critical ecological connectivity, a prerequisite for reconciling large-scale renewable energy deployment with biodiversity conservation imperatives. Operational implementation should integrate real-time turbine wake modelling with bird movement telemetry for dynamic zone boundary calibration.

Strategic placement of turbines to reduce the impact wakes on bird flight aerodynamic effects

The spatial configuration of wind turbines within offshore wind farms is of critical importance in determining both energy capture efficiency and ecological impact mitigation. The strategic placement of turbines not only enhances individual turbine performance by minimizing wake impact but also fundamentally alters wake distribution pattern, which is the key determinant of aerodynamic risks to bird flight.

We demonstrate that staggered turbine configurations significantly modify wake-induced aerodynamic impacts on birds. Through numerical simulations under neutral atmospheric stability, four lateral displacement scenarios (0D, 0.5D, 1D, and 1.5D, where D is rotor diameter) are analyzed. X-Y plane visualization wake induced impact on bird flight performance (Fig. 6) reveals progressive risk reduction with increasing staggered offsets:

0D alignment: Extensive high-risk zones (red, $\Delta K/K_0 > 0\%$) persist across multiple turbine rows, particularly in top tip level.

0.5D displacement: The red high-risk areas for the first two turbines have almost disappeared, and the extent of the red high-risk areas for the subsequent turbines has been reduced to varying degrees.

1D offset: The area encompassing the yellow, more hazardous zones, and the red, high hazard areas, is diminishing at a rapid rate. Presently, only a few clearly visible yellow areas remain behind a few turbines.

1.5D staggering: It is evident that the initial three turbines have minimal coverage of the yellow areas. Additionally, the red areas, categorized as high hazard, have almost disappeared from the overall wake area.

In summary, the implementation of staggered turbine placement in wind farms has significant benefits in reducing bird flight hazard zones. It is evident that the greater the distance of the staggered arrangement, the more pronounced the effect. It can thus be concluded that the implementation of staggered arrangements has the potential to reduce the coverage of dangerous areas in the wake of wind farms. In particular, the scope of the red high-danger areas can be effectively reduced by establishing a reasonable staggered distance. This, in turn, will effectively reduce the impact of turbine wakes on the bird flight aerodynamic effects.

Discussion

The impacts of wind turbine wake on bird flight are investigated by employing LES and RANS. The numerical results indicate that turbulence intensity is the primary factor affecting the flight performance of birds in the wake of a wind turbine. The results reveal how wind turbine wakes affect bird flight behaviors at different positions. The influences on bird flight are greatest at downstream (4 diameters of turbine rotor). The area at the top of the wind turbine exerts the most significant impact, where the lift-to-drag ratio (K) of the birds' flight can be reduced by 30%. Between the hub centre and the lower tip, the reduction in the K is relatively minor. It is noteworthy that between the sea surface and the lower tip, the wake has a positive effect on elevating the K with a rise of 10–15%. This can be regarded as a assistant channel for birds' flights, and it could be advantageous to birds flying.

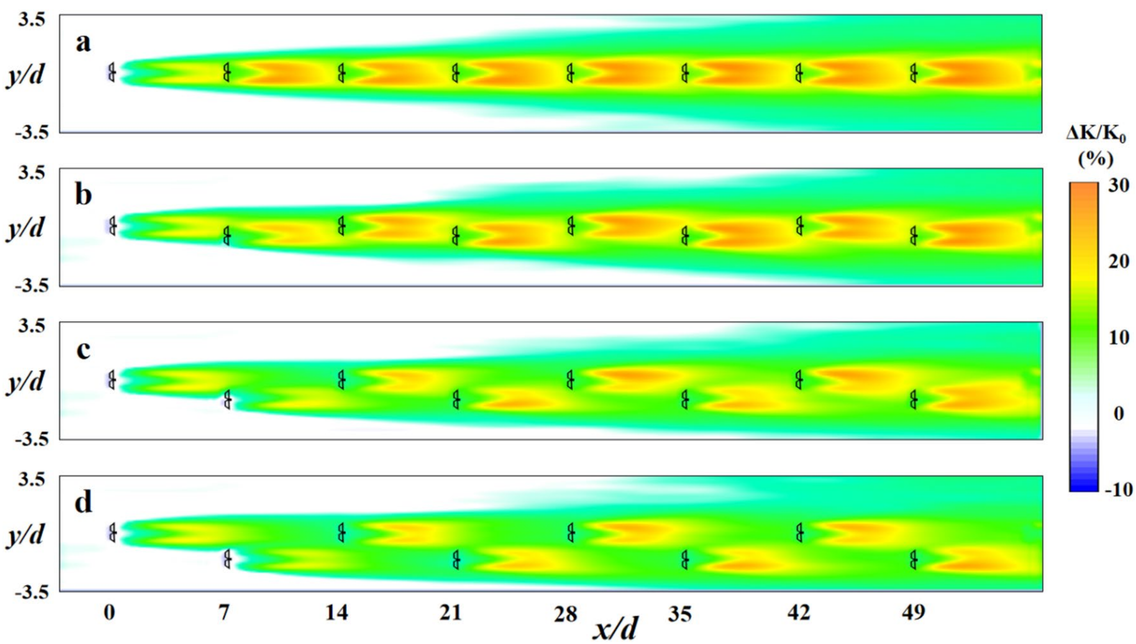

Fig. 6. Distribution of the rate of change of lift-to-drag ratio $|\Delta K/K_0|$ in the hub-height y-z section in turbine array condition at different mismatch distances: (a) mismatch distance 0 D (b) mismatch distance 0.5 D (c) mismatch distance 1 D (d) mismatch distance 1.5 D.

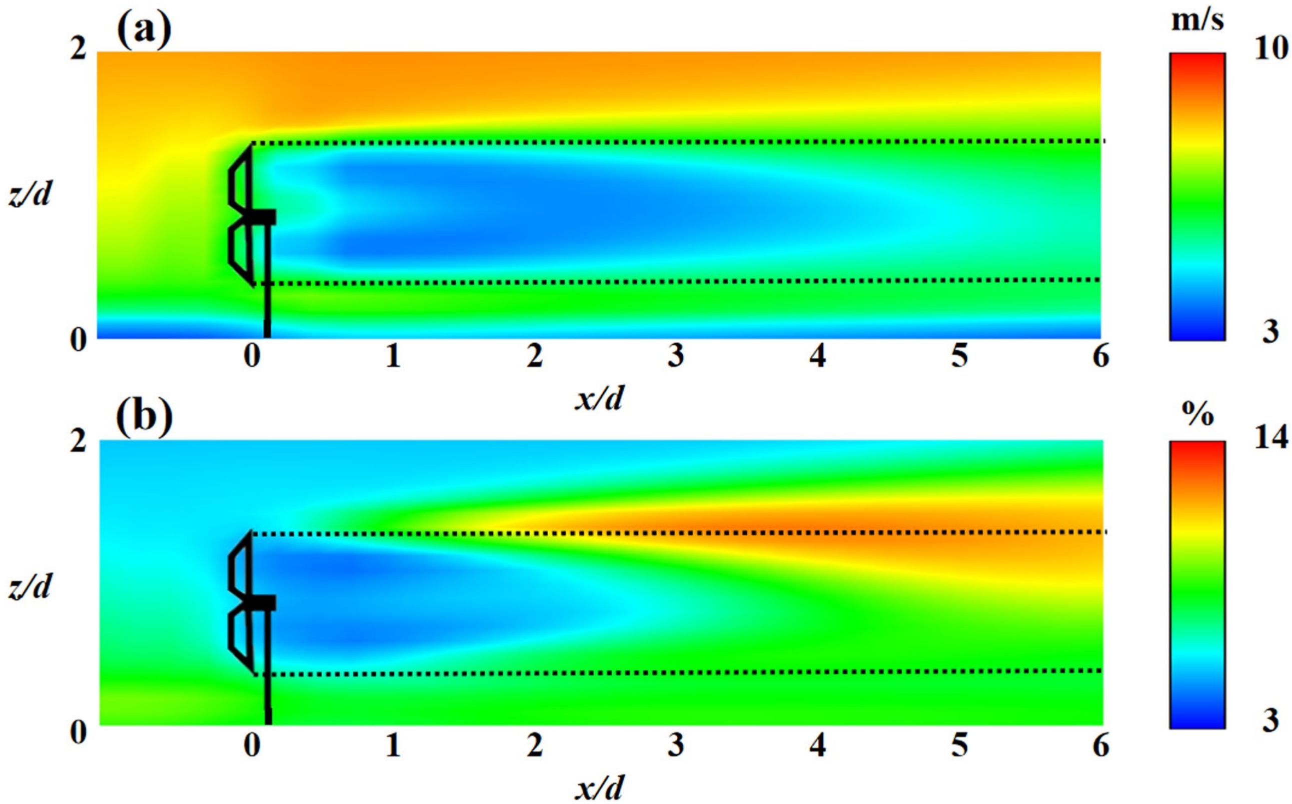

Fig. 7. Distribution of mean flow velocity (a) and turbulence intensity, (b) for the x-z section at the centre of the computational domain.

As a significant improvement to previous observations and statistical methods, our study employs numerical simulation for the first time to investigate the impacts of wind turbine wakes on bird flight. Furthermore, a comprehensive analysis of the impacts is presented. A formula of K of bird flight is presented based on the numerical results. This may facilitate the rational deployment and control of the corresponding protection equipment, such as bird repellents and reflectors. The results indicate that the optimal protection area for birds is the region near the upper tip height, while the area below the lower tip requires minimal protection measures.

Wake superposition exacerbates adverse aerodynamic effects. Staggered turbines in wind farms can significantly reduce the hazard zone for bird flight, while at the same time providing significant benefits in terms of increasing the amount of electricity generated by the wind farm. Therefore, the interests of maximizing energy production and assisting bird flight coincide in this aspect of avoiding the effects of wake turbulence.

Current research has only considered the simple scenario of gliding flight in birds and has only examined atmospheric inflow conditions under neutral stability. Future research will explore more complex bird flight states, such as flapping scenarios and flexible wing deformation, while also investigating the effects of different atmospheric inflow conditions, such as stable atmospheric boundary layers and convective atmospheric boundary layers. Additionally, more extreme scenarios, such as high wind speeds and turbulent intensity will be considered. Despite its simplifications, this framework successfully identifies specific high-risk zones within the wake. This spatial map of aerodynamic hazard provides valuable, previously unavailable data for ecological risk assessments and can inform wind farm layout planning to minimize potential conflicts, even in the absence of vastly more complex and computationally expensive fully-coupled simulations.

Methods

LES of wind turbine wakes

The prototype employed in this study is a 2 MW wind turbine situated within the Horn Rev offshore wind farm. This has been the subject of extensive research, with a substantial corpus of measured data and high-fidelity LES data available for reference[25–28]. This paper is based on the widely used coupled scheme of the rotating actuator disc model (ADM-R) and large eddy simulation (LES) for simulating and solving the turbine wake[25–31]. A substantial amount of evidence demonstrates that this simulation method can yield highly accurate information about the wake field. The simulations are conducted using the commercial software FLUENT (Ansys fluent version 17.0 https://www.ansys.com/), with the LES of the flow fields based on the Smagorinsky Lilly model incorporated[32]. The rotating disc model code of the wind turbine has been developed using the UDF, with the reaction force of wind turbines in the form of a volumetric force source term. Further details regarding the rotating actuator disc model and the LES of turbine wakes can be found in our previous work[28].

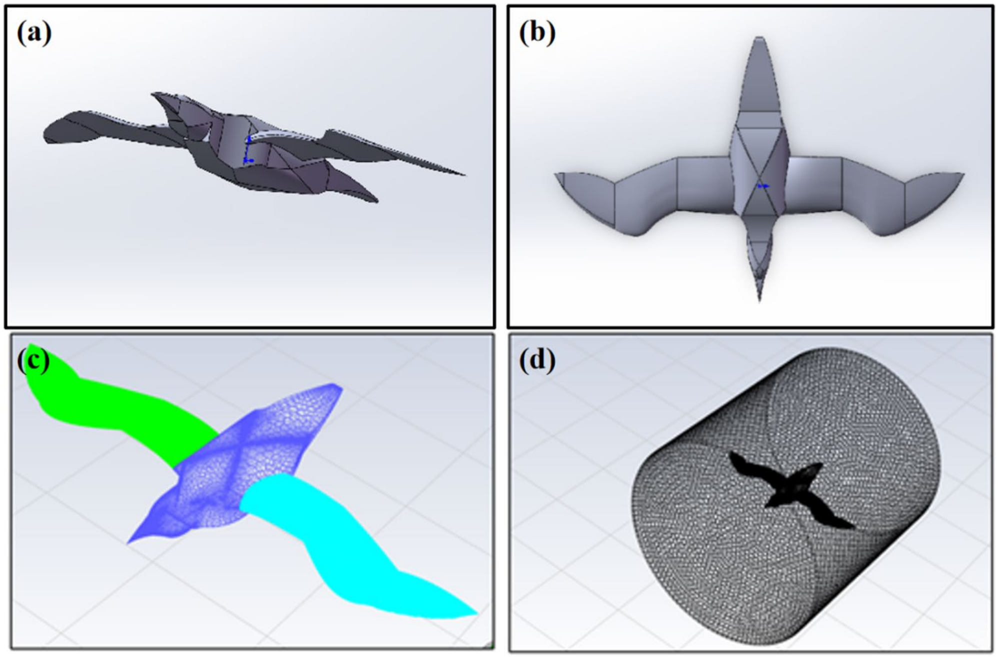

Fig. 8. Red-footed booby model and the flow field grid for bird flight simulation.

RANS simulation of bird flight

Wind tunnel experiments[33–35] and numerical simulations[34–40] are widely used in the study of bird flight.Referring to previous research methods[37–39], this paper use numerical simulation methods to simulate the flight conditions of birds at different wake positions. This paper employs the FLUENT software[41,42] to simulate the flight process of birds, with the red-footed booby selected as the modelling object. This species is afforded the status of a second-class protected animal in China, with a predominantly tropical distribution and a high population density in the South China Sea. The morphology of the red-footed booby was modelled in a reductive manner, utilizing data from the National Taxidermy Resource Bank, isometric photographs and pertinent anatomical literature. Solidworks is exclusively employed for geometric modeling of the bird form. (Fig. 8). The pre-processing of the model is conducted with Spaceclaim. The external flow field is created by extracting the corresponding fluid domain via Boolean subtraction (Fig. 8). Subsequently, Fluent Meshing generates the mesh. The flow parameters of the turbine wake (Fig. 1) are imported into bird flight simulation case as the velocity boundary conditions and are solved based on the Reynolds-Averaged Navier-Stokes (RANS) turbulence model. The built-in monitors are then used to monitor the lift, drag, and the characteristics of the external flow field of the bird. Subsequently, sensitivity experiments are conducted in Fluent for each flow field parameter under a uniform flow field, with parameters such as flow velocity and turbulence intensity.

Within the current simulation framework, the modeled bird maintains zero ground-relative velocity while flying at a constant airspeed equivalent to the local wind turbine wake velocity. A limitation of our model is that the imposed zero ground-speed condition leads to a variable and often unrealistically low bird airspeed, which does not reflect the tendency of birds to fly at a consistent airspeed. Future models should incorporate active flight control strategies to maintain a constant and higher airspeed, which would provide a more accurate representation of bird flight behavior through wind farms. The bird model is aligned solely with the streamwise (u) component of the flow. The vertical (w) and lateral (v) velocity components from the LES are not incorporated into the RANS inflow conditions. This omission may lead to an underestimation of aerodynamic effects, particularly in regions with strong vertical flow. The angle of attack is maintained at 0°. A primary limitation of this work is the use of a static, gliding model. It does not capture the complex, unsteady aerodynamics of flapping flight, such as leading-edge vortex formation, which can generate transient lift forces far exceeding those in gliding. Consequently, our results are strictly applicable to gliding or soaring transit and should not be extrapolated to flapping flight. More detailed information about the bird model and the RANS setting can be found from the Supporting information.

The most crucial issue is that of establishing a quantitative methodology for the description of the impacts on birds. A physical quantity is required to provide an intuitive measure of the extent of the impact on bird flight. A review of the literature reveals that the majority of studies employ the lift coefficient C_l, the drag coefficient C_d, and the lift-drag ratio K, which is defined as the ratio of the lift coefficient to the drag coefficient. Consequently, this paper proposes the use of the lift-drag ratio, which represents the ratio of the lift and drag forces acting on the bird in the flow field, as a means of quantifying the aerodynamic performance of bird flight. The expression is as follows:

$$C_l = \frac{L}{\frac{1}{2}\rho V^2 S} \tag{4}$$

$$C_d = \frac{D}{\frac{1}{2}\rho V^2 S} \tag{5}$$

$$K = \frac{C_l}{C_d}, \tag{6}$$

where L represents the lift force acting on the bird, D denotes the drag force experienced by the bird, ρ signifies the air density, V stands for the relative flow velocity, and S refers to the reference area. The lift coefficient and drag coefficient reflect the dimensionless magnitude of the lift and drag forces exerted on the bird during flight, and are employed to assess the bird's lift performance and drag performance. In contrast, the lift-to-drag ratio provides a quantitative description of the bird's aerodynamic performance. Typically, a larger lift-to-drag ratio indicates enhanced lift performance and increased aerodynamic efficiency. The lift-to-drag ratio (K) serves solely as an indicator of aerodynamic efficiency, reflecting flight difficulty rather than directly equating to survival safety.

Data availability

Data is provided within the manuscript or supplementary information files, but also upon request from the authors (yxf22@mails.tsinghua.edu.cn).

Received: 15 May 2025; Accepted: 15 December 2025
Published online: 19 December 2025

References

1. Council, G. W. E. GWEC global wind report 2024. In *Global Wind Energy Council: Bonn, Germany* (2024).
2. Subramanian, M. An ill wind. *Natures* **486**, 310 (2012).
3. Wang, S., Wang, S. & Smith, P. Ecological impacts of wind farms on birds: questions, hypotheses, and research needs. *Renew. Sustain. Energy Rev.* **44**, 599–607 (2015).
4. Manville, A. M. Towers, turbines, power lines, and buildings–steps being taken by the US Fish and Wildlife Service to avoid or minimize take of migratory birds at these structures. In *Proceedings of the Fourth International Partners in Flight Conference: Tundra to Tropics, vol. 18* 262272 (2009).
5. Sovacool, B. K. The avian benefits of wind energy: a 2009 update. *Renew. Energy*. **49**, 19–24 (2012).
6. Smallwood, K. S. Comparing bird and Bat fatality-rate estimates among North American wind-energy projects. *Wildl. Soc. Bull.* **37**, 19–33 (2013).
7. Loss, S. R., Will, T. & Marra, P. P. Estimates of bird collision mortality at wind facilities in the contiguous united States. *Biol. Conserv.* **168**, 201–209 (2013).
8. Bech, M., Frederiksen, R., Pedersen, J. & Leonhard, S. B. Infauna monitoring. Horns Rev Wind Farm 2004. Status Report. In *Prep. Report request. Commissioned by Elsam Engineering A/S* (2005).
9. Pettersson, J. & Stalin T. Influence of offshore windmills on migration birds in southeast coast of Sweden. Report to GE Wind Energy. (2003).
10. Brown, M. J., Linton, E. & Rees, E. C. Causes of mortality among wild swans in Britain. *Wildfowl* **43**, 70–79 (1992).
11. Alerstam, T. *Bird Migration* (Cambridge University Press, 1993).
12. ZERVOS, A. Wind energy the facts. *European Wind Energy Association (EWEA) Belgium* 83–85 (2009).
13. Thelander, C. G., Smallwood, K. S. & Rugge, L. *Bird Risk Behaviors and Fatalities at the Altamont Pass Wind Resource Area: March 1998-December 2000. Period of Performance* (National Renewable Energy Laboratory, 2003).
14. de Lucas, M., Janss, G. F. & Ferrer, M. Birds and wind farms. *Quercus Madrid* (2007).
15. Dahl, E. L. et al. White-tailed eagles (Haliaeetus albicilla) at the Smøla wind-power plant, central Norway, lack behavioral flight responses to wind turbines. *Wildl. Soc. Bull.* **37**, 66–74 (2013).
16. Furness, R. W., Wade, H. M. & Masden, E. A. Assessing vulnerability of marine bird populations to offshore wind farms. *J. Environ. Manage.* **119**, 56–66 (2013).
17. Janss, G. F. Avian mortality from power lines: a morphologic approach of a species-specific mortality. *Biol. Conserv.* **95**, 353–359 (2000).
18. Jenkins, A. R. et al. Combining radar and direct observation to estimate pelican collision risk at a proposed wind farm on the cape West coast, South Africa. *PloS One*. **13**, e0192515 (2018).
19. de Lucas, M., Ferrer, M. & Janss, G. F. Using wind tunnels to predict bird mortality in wind farms: the case of griffon vultures. *PloS One*. **7**, e48092 (2012).
20. Therkildsen, O. R. et al. D. Changes in flight paths of large-bodied birds after construction of large terrestrial wind turbines. *J. Environ. Manage.* **290**, 112647 (2021).
21. Bolker, E. D., Hatch, J. J. & Zara, C. Modeling how windfarm geometry affects bird mortality. *arxiv preprint arxiv:1408.1580* (2014).
22. Stokke, B. G., Nygård, T., Falkdalen, U., Pedersen, H. C. & May, R. Effect of tower base painting on Willow ptarmigan collision rates with wind turbines. *Ecol. Evol.* **10**, 5670–5679 (2020).
23. Therkildsen, O. R., Elmeros, M., Kahlert, J. A. & Desholm, M. Baseline investigations of bats and birds at Wind Turbine Test Centre Østerild. Scientific Report from DCE-Danish Centre for Environment and Energy. Aarhus University, Department of Bioscience, Denmark (2012).
24. Therkildsen, O. R. & Elmeros, M. Second year post-construction monitoring of bats and birds at Wind Turbine Test and no.: Scientific Report from DCE–Danish Centre for Environment and Energy (2017).
25. Wu, Y. T. & Porté-Agel, F. Simulation of turbulent flow inside and above wind farms: model validation and layout effects. *Bound. Layer Meteorol.* **146**, 181–205 (2013).
26. Wu, Y. T. & Porté-Agel, F. Modeling turbine wakes and power losses within a wind farm using LES: an application to the Horns rev offshore wind farm. *Renew. Energy*. **75**, 945–955 (2015).
27. Ti, Z., Deng, X. W. & Yang, H. Wake modeling of wind turbines using machine learning. *Appl. Energy*. **257**, 114025 (2020).
28. Yang, X. et al. A numerical study of rainfall effects on wind turbine wakes. *Renew. Energy* **2024**, 120801 (2024).
29. Yang, H., Ge, M., Gu, B., Du, B. & Liu, Y. The effect of swell on marine atmospheric boundary layer and the operation of an offshore wind turbine. *Energy* **244**, 123200 (2022).
30. Yang, H., Ge, M., Abkar, M. & Yang, X. I. Large-eddy simulation study of wind turbine array above swell sea. *Energy* **256**, 124674 (2022).
31. Ishihara, T. & Qian, G. W.A new Gaussian-based analytical wake model for wind turbines considering ambient turbulence intensities and thrust coefficient effects. *J. Wind Eng. Ind. Aerodyn.* **177**, 275–292 (2018).
32. Smagorinsky, J. General circulation experiments with the primitive equations. *Mon Weather Rev.* **91**, 99–164 (1963).

33. Tucker, V. A. & Parrott, G. C. Aerodynamics of gliding flight in a Falcon and other birds. *J. Exp. Biol.* **52**, 345–367 (1970).
34. Rosén, M. & Hedenström, A. Gliding flight in a jackdaw: a wind tunnel study. *J. Exp. Biol.* **204**, 1153–1166 (2001).
35. Spedding, G. R., Hedenström, A. & Rosén, M. Quantitative studies of the wakes of freely flying birds in a low-turbulence wind tunnel. *Exp. Fluids*. **34**, 291–303 (2003).
36. Zhu, Q. Numerical simulation of a flapping foil with chordwise or Spanwise flexibility. *AIAA J.* **45**, 2448–2457 (2007).
37. Muijres, F. T., Bowlin, M. S., Johansson, L. C. & Hedenström, A. Vortex wake, downwash distribution, aerodynamic performance and wing beat kinematics in slow-flying pied flycatchers. *J. R. Soc. Interface* **9**, 292–303 (2012).
38. Beaumont, F., Bogard, F., Murer, S. & Matim, P. G. Modeling of three-dimensional unsteady wake past a large migratory bird during flapping flight. *WSEAS Trans. Fluid Mech.* **17**, 10–17 (2022).
39. Soni, A. & Tiwari, S. Three-dimensional numerical study on aerodynamics of non-flapping bird flight. *Sādhanā* **44**, 1–15 (2019).
40. Wang, L. & Tian, F. B. Numerical study of flexible flapping wings with an immersed boundary method: Fluid-structure-acoustics interaction. *J. Fluids Struct.* **90**, 396–409 (2019).
41. Ferziger, J. H., Perić, M. & Street, R. L. *Computational Methods for Fluid Dynamics* (Springer, 2019).
42. Inc, A. ANSYS fluent 18.0 user's guide (2017).

Acknowledgements
This study is supported by funds from National Key R&D Program of China (2024YFC3013201), Shenzhen Science and Technology Innovation Committee (KCXFZ20240903093900002), and Guangdong Basic and Applied Basic Research Foundation (2022B1515130006). Y Sui is funded by the China Postdoctoral Science Foundation (2024M761611).

Author contributions
X. Y. and L. Z. were responsible for the numerical simulaion and data collection. X. Y. and L. Z. wrote the main manuscript text. Y. S., Z. R. and S. Z. gave advice and support. All authors reviewed the manuscript.

Funding
Open Access funding enabled and organized by Guangdong Basic and Applied Basic Research Foundation.

Competing interests
The authors declare no competing interests.

Additional information
Supplementary Information The online version contains supplementary material available at https://doi.org/10.1038/s41598-025-33055-x.

Correspondence and requests for materials should be addressed to S.C.